SEMARAK ILMU PUBLISHING

CFD Letters

Journal homepage:
https://semarakilmu.com.my/journals/index.php/CFD_Letters/index
ISSN: 2180-1363

Numerical Investigation of the Power Performance of the Vertical-Axis Wind Turbine with Endplates

Chun Khai Tan[1,*], Ahmad Faiz Mohammad[1], Ahmad Fazlizan[2], Sheikh Ahmad Zaki[1], Farah Liana Mohd Redzuan[1]

[1] Malaysia-Japan International Institute of Technology, Universiti Teknologi Malaysia, Jalan Sultan Yahya Petra, 54100 Kuala Lumpur, Malaysia
[2] Solar Energy Research Institute, Universiti Kebangsaan Malaysia, 43600 Bangi, Selangor, Malaysia

ARTICLE INFO

Article history:
Received 20 April 2022
Received in revised form 8 June 2022
Accepted 9 June 2022
Available online 30 June 2022

Keywords:
VAWT; CFD; Endplates

ABSTRACT

An H-rotor vertical axis wind turbine (VAWTs) can operate independently in any wind direction, making it aerodynamically efficient and suitable to harness wind energy in low wind speed areas. The aerodynamic efficiency of VAWTs is highly dependent on the blade geometry, especially the blade tip. Tip vortices produced at the blade tips can negatively affect the VAWT's aerodynamic efficiency. Adding endplates to the blade tips can minimize the effects of tip vortices on VAWTs. In this paper, several endplate designs are used to evaluate the effectiveness in improving the power coefficient, C_p of a VAWT at three different tip speed ratios (*TSR*s) using three-dimensional computational fluid dynamics (3D CFD) simulation. The power coefficients of VAWTs with endplates are compared with the baseline model with the same geometrical parameters where the baseline VAWT model is based on the experimental model from the literature. Since the focus of this study is on the blade tip design, a simplified 3D VAWT model is used where the supporting shaft and arms of the VAWT are excluded to reduce the needed computational capacity. Among the various endplate designs used in this study, the semi-circular inward endplate (ED3) with a diameter equivalent to 1.2 blade chord length showed the best improvement in the *Cp* which is by 7.45%, and 5.79% for at the *TSR*s of 2.19 and 2.58, respectively. The pressure difference on both sides of the blade was also examined. The results revealed that the endplate can prevent the flow from bypassing the blade tip, hence, preventing the occurrence of tip vortices while improving the aerodynamic efficiency near the blade tip, ultimately, improving the overall C_p of a VAWT.

1. Introduction

The severity of global warming and climate change urge energy sectors to replace fossil fuels with renewable energies as energy sources. Wind energy is one of the clean energies due to its availability across the globe [1, 2]. Recently, in the efforts to increase wind energy generation, vertical-axis wind turbines (VAWTs) have gained widespread attention due to the omni-directional characteristic that makes them ideal for small-scale energy generation in urban environments [3-5]. Studies from

* *Corresponding author.*
E-mail address: cktan513@gmail.com (Chun Khai Tan)

https://doi.org/10.37934/cfdl.14.6.90101

Nofirman *et al.,* [6] revealed that VAWTs are more suitable to be used in urban application when multiple turbines are installed on a building. Researchers have also started to explore the possibility to recover wind energy from the exhaust air [7].

The performance of a VAWT is affected by various factors, one of which is the tip vortex shedding effect. The effect of tip vortex shedding on the performance of a VAWT is confirmed by Li *et al.,* [8] where the authors noticed that the discrepancy between the 2.5D CFD study and the experimental results grew wider as the cross-sectional torque coefficient analysis moved towards the blade tip. Studies revealed that tip vortices occur intensely at a distance of about two-chord length from the blade tip [9, 10]. Thus, the tangential force becomes unevenly distributed along the blade span due to the induced drag created by the tip vortices.

Several attempts have been made by researchers to improve the VAWT efficiency by minimizing the impact of tip vortices on the turbine blade. One of the most effective methods is by adding endplates to the blade [9, 11-19]. An endplate is a thin piece of object that is attached to the end tip to minimize the end tip leakage vortex by preventing the air from the high-pressure side from bypassing. It has been applied in many applications. The most prominent application is on the aircraft where the endplate is used to minimize the strength of the trailing edge vortex and to reduce the induced drag in the aircraft wing [20]. For the application on an aircraft, it has been reported that the endplate increased the lift-drag ratio when the angle of attack is positive [21].

Mishra *et al.,* [14] used a three-bladed VAWT to evaluate the endplate size with 15 mm offset and 25 mm offset. The endplates are made from the NACA 0018 profile, which is the same profile as the blade, and it was tested for the tip speed ratio, *TSR* ranging between 0.25 to 0.8. The authors reported that the 15 mm offset endplate showed a better improvement in power efficiency. Similarly, Jiang *et al.,* [22] evaluated five different sizes of endplate on a large-scale single-bladed VAWT at the *TSR* of 3. The endplate sizes were manipulated based on the edge distance between the endplate and the blade surface. It was concluded that the distance equivalent to 0.35 times the blade chord length, *c*, is the preferred distance. With this endplate size, the total torque of the blade was increased by 4.25%. However, it was reported by Gosselin *et al.,* [9] that the large circular endplate is unable to improve the power performance although it is able to normalize the pressure distribution on the blade surface. On the other hand, Yamada *et al.,* [17] investigated the endplates installation angles between -90°, -45°, + 45°, and + 90°. Amongst these installation angles, it was reported that the endplates positioned at -90° showed the best improvement in the VAWT power efficiency. However, none of these installation angles were able to improve the VAWT power efficiency when the operating conditions go below the *TSR* of 0.87.

Although the endplate indeed improves the power performance of a VAWT, the effects of the endplate designs are not sufficiently studied. Therefore, the endplate profile effects need to be further investigated to determine its optimum design.

2. VAWT Model and Operational Parameters

The geometrical parameters of the H-rotor VAWT model in these studies were based on the rotor specifications used in the wind tunnel study of Li *et al.,* [23]. The rotor blade is made from NACA 0021 profile with a chord length, *c* of 0.265 m, a blade span of 1.2 m, and the blade is set to a +6° pitch angle. It is a two-bladed rotor with a rotor diameter, *D* of 2 m. The rotor solidity is 1.06, which is defined as *Nc*/*D*, where *N* is the number of blades, *c* is the chord length, and *D* is the rotor diameter. The geometrical model is shown in Figure 1(a).

According to Li *et al.,* [23], the VAWT model was tested at three different tip speed ratios ($TSR = \omega R/U_\infty$), which are *TSR* = 1.38 (low tip speed ratio), 2.19 (optimum tip speed ratio), and 2.58 (high tip speed ratio).

3. Simulation Model Introduction

Since the 3D CFD simulation in this study is focused on the blade tip effect, the modeled mechanism of the rotor was simplified where the shaft and strut of the rotor were excluded. Besides, the symmetrical approach was adopted in these studies to further reduce the computational time because the upper rotor and the lower rotor are identical. The computational domain is partitioned into two regions, rotor and stator. As shown in Figure 1(b), the stator domain size was a rectangular tunnel with 10*D* (width) x 5*D* (height) x 25*D* (length) and the rotor domain size was a cylinder with a diameter of 1.5*D* and height of 1 m. The rotor has 10*D* upstream distance from the inlet and 15*D* downstream distance from the outlet. At the domain inlet, the experimental inlet velocity (U_∞) of 8 m/s was set and the pressure outlet with a value of 0 Pa was used. The remaining four boundaries surrounding the stator were assigned as symmetry conditions. For the surfaces between the stator and the rotor, an interface boundary condition was employed to allow a smooth flow between these two domains. Lastly, a no-slip wall boundary condition was applied to the blade surfaces.

The unstructured mesh approach was used for the entire computational domain. According to literature, the *y*+ (dimensionless wall distance) of less than 5 is commonly used in the 3D CFD simulation of VAWTs where it is sufficient to capture the viscous sub-layer boundary layer effect [24-27]. Therefore, the first cell thickness on the blade walls was set to 3 x 10^{-5} m with 30 layers at a thickness growth rate of 1.2.

The sliding mesh technique was applied to allow mass and momentum exchange among the cells between the stator domain and rotor domain. Besides, the mesh sizes on the surfaces between the stator domain and rotor domain were identical to ensure a smooth transition from one domain to another. To provide acceptable computational accuracy, the azimuthal time step of 1° was applied in the CFD simulations of this study, based on the CFD study of Wong *et al.,* [24] validated with Li et al. [17].

The convergence of the simulation is based on the time history of the power coefficient, C_p over one revolution of the VAWT. When the C_p of the two successive revolutions shows a discrepancy lower than 1%, the solution is considered converged.

The selection of the turbulence model was based on the comparison of various RANS turbulence models conducted by Wong *et al.,* [24]. From the comparison, the author concluded SST *k*-*ω* provides the closest match with respect to the experimental data obtained by Li *et al.,* [23]; this was also confirmed by other researchers [28, 29]. Therefore, SST *k*-*ω* is used in this study. Moreover, a pressure-based solver with the SIMPLE scheme was selected, similar to the setting used by Wong *et al.,* [30]. It is commonly employed in CFD simulations for VAWTs due to its low computational cost and result accuracy [31].

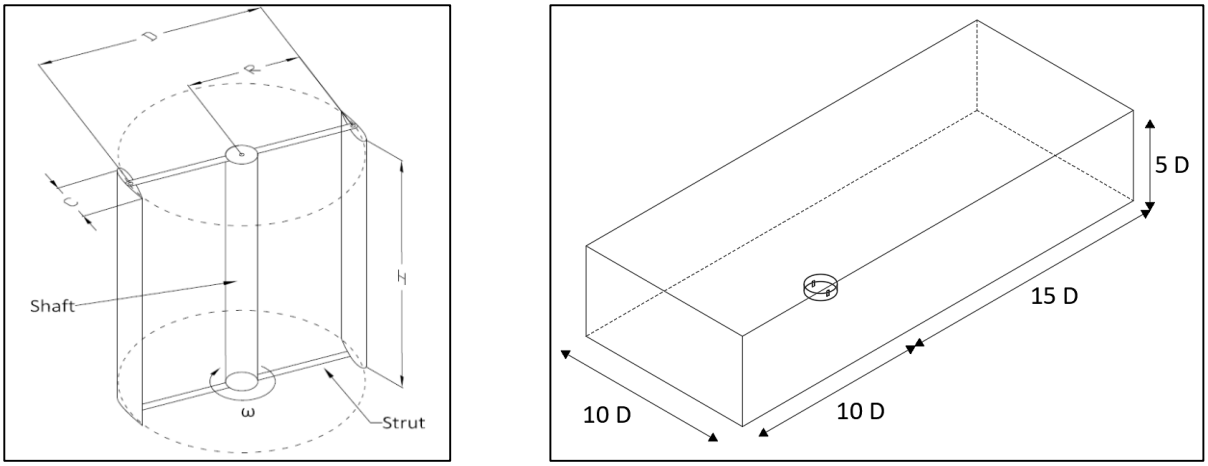

(a) (b)

Fig. 1. (a) Geometrical illustration of the VAWT (b) Computational domain

4. Results

The performance of the VAWT is compared by evaluating the C_p which is defined in Eq. (1).

$$Cp = \frac{P}{0.5\rho A U_{\infty}^{3}} \tag{1}$$

where, *P* represents the power generated, *ρ* is the air density, and *A* is the area of the VAWT. The comparison was done for three tip speed ratios ($TSR = \omega R/U_{\infty}$), which are 1.38, 2.19, and 2.58.

4.1 Simulation Validation

The wind tunnel test data published by Li *et al.,* [23] were used for validation. The *Cp* at one of the blades for these cases at various azimuthal angles (θ) for a complete cycle is shown in Figure 2. The peaks of the C_p obtained from the simulation are 0.382, 0.594, and 0.65 whereas the experimental data are 0.419, 0.517, and 0.613 for the *TSR*s of 1.38, 2.19, and 2.58, respectively. The small difference in the peak C_p between the simulation and experimental data is due to the geometrical simplification between the simulation model and the experimental model [32, 33].

Figure 2 shows that the C_p trend from the simulation shows good agreement with the experimental data for all three *TSR*s, especially in the upwind region (45° ≤ θ ≤ 135°). Nevertheless, there are some differences in the region 225° ≤ θ ≤ -30° between the simulation results and the experimental data, as reported by Li *et al.,* [8]. This is because the flow field at this region is complex due to blade-wake interaction [34]. The differences are more severe for the *TSR* of 1.38 where the CFD unable to detect the second peak as per the experimental measurements. This is because CFD simulation is unable to exactly evaluate the pressure distribution to the lower analysis accuracy in dynamic stall [8, 29]. Furthermore, the same trends were reported by other researchers who use the similar NACA airfoil series [33, 35-37]. Furthermore, the CFD data obtained were also compared with the CFD data reported by Wong *et al.,* [30], revealing close similarity. Generally, the comparison indicates that the numerical settings and boundary conditions applied in this work are able to produce comparable results with the published data.

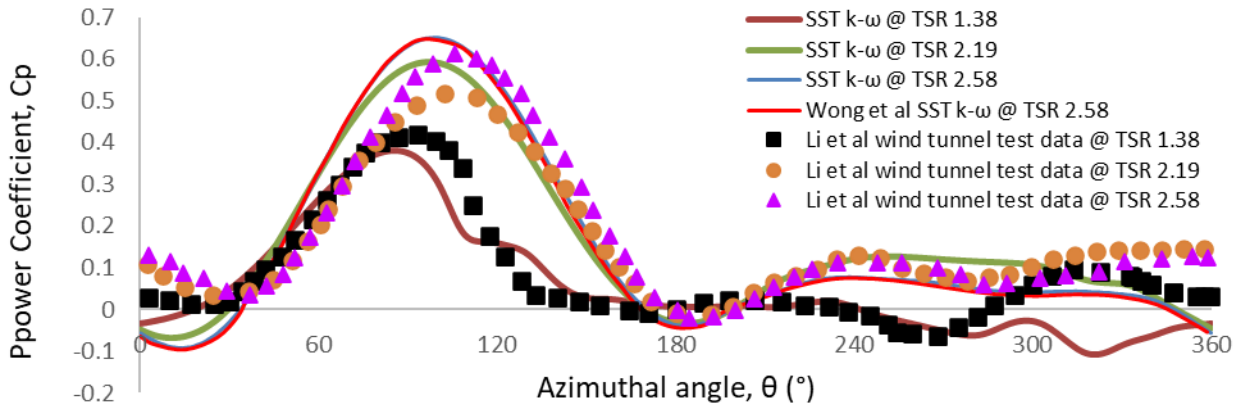

Fig. 2. Comparison of C_p for the single-bladed VAWT between the simulation data and the wind tunnel test data for a complete revolution at *TSR*s of 1.38, 2.19, and 2.58

4.2 Effects of Endplate

To investigate the effects of endplate on the performance of VAWT, the same geometry of VAWT that was used in the validation studies is applied. Four different endplate designs based on NACA 0030 (ED1), circular profiles (ED2), semi-circular inward (ED3), and semi-circular outward (ED4) each with a thickness of 1 mm, were used. The endplate designs are shown in Figure 3. For comparison, the blade span is maintained. The evaluation was done at *TSR*s of 1.38, 2.19, and 2.58.

The effects of the endplate on the C_p of VAWT are summarised in Table 1. The results showed that none of the endplate designs were able to improve the performance at the *TSR* of 1.38. Amongst those, ED2 yields the most dropped in performance, which is a reduction of 31.16 % when compared to the baseline. However, the power performance calculated by CFD at a low *TSR* should be treated with caution due to a large angle of attack (AOA) variation at a low *TSR* which results in dynamic stall, and it is difficult to be captured accurately in CFD [38, 39].

As for the *TSR*s of 2.19 and 2.58, ED2, ED3, and ED4 all showed improvement in the C_p. Amongst these three designs, ED3 delivers the most promising results, which improve the C_p by 7.45% at the *TSR* of 2.19 and 5.79% at the *TSR* of 2.58. On the other hand, ED2 only shows significant improvement at the *TSR* of 2.58, where the C_p is improved by 7.21%. Whereas ED4 showed insignificant improvement at the *TSR*s of 2.19 and 2.58, which is merely 1.75% and 0.42% respectively. On the contrary, ED1 worsens the C_p at the *TSR*s of 2.19 and 2.58 when compared with the blade without an endplate.

To further understand the performance of VAWT with endplate, the instantaneous C_p over one revolution of a blade for each case is analysed. The summary of C_p for blade 1 is tabulated in Table 2 and the instantaneous C_p is shown in Figures 4 (a), 4 (b), and 4 (c) which represent the operating conditions with the *TSR*s of 1.38, 2.19, and 2.58, respectively. A positive value of instantaneous C_p represents the blade producing useful energy whereas a negative value of instantaneous C_p represents the blade consuming the energy which gives a negative impact on the overall C_p. As can be seen from the graphs, the blade with endplates shows higher amplitude, which means endplates increase not only the positive power but also the negative power at some azimuthal angles.

As shown in Figure 4 (a), useful energy is only produced in the region between $20° \leq \theta \leq 126°$ for the *TSR* of 1.38. When endplates are added, additional drag is added which makes the blades

consume extra energy to move in the non-energy producing region. This explains that endplates are unable to improve the C_p at the *TSR* of 1.38.

On the other hand, the positive C_p region for the *TSR*s of 2.19 and 2.58 is much wider and the negative C_p region is much narrower compared to the *TSR* of 1.38. This is because the AOA is smaller at higher *TSR*s, hence delaying the occurrence of dynamic stall, allowing lift to be produced for a wider region [34]. At the *TSR* of 2.19, although ED2 improved the peak C_p by 13.89% compared to ED3 which only improved the peak C_p by 12.60%, ED2 showed a higher average negative region than ED3. Thus, ED3 delivers better improvement overall. Whereas for *TSR* 2.58, ED2 improved the peak C_p by 14.43% compared to ED3 which only improved the peak C_p by 11.83%. However, the average gain for ED2 in the positive region is more than ED3, hence, it managed to counter the loss in the negative region, making ED2 stand out in the overall performance.

The pressure distribution for a blade at 90° where the VAWT is operating at the *TSR* of 2.58 is illustrated in Figure 5. The pressure distribution on both sides of the blade surfaces represents the amount of lift generated on each section. As noticed, endplates help in redistributing the flow condition along the blade span. In Figure 5(a) where the endplate is not attached to the blade tip, the surface pressure near the blade was distorted due to the presence of blade tip vortices. ED2 showed the greatest pressure redistribution which explained that ED2 yields the highest C_p in Figure 4(c). The increase in positive power is due to the successful suppression of tip vortices which increases the power generation near the blade tip. Therefore, the induced drag was reduced, and the blade aerodynamic performance was improved [38, 40].

Between ED3 and ED4, the pressure distribution contours revealed that the endplate should be facing inward in order to effectively minimize the blade tip loss. The pressure distribution contour on the low-pressure side for ED4 (Figure 5 (f)) is almost identical to the blade without an endplate (Figure 5 (a)). This explained that ED4 did not show a significant improvement in the C_p compared to the blade without an endplate.

Although Figure 5 (b) shows that ED1 did help in redistributing the pressure near the blade tip, it did not show improvement in the overall C_p. The energy recovered from the blade tip loss was lesser than the additional drag created by ED1. This can be interpreted from the positive region C_p in Table 2. Indeed, the energy generation in the positive region when ED1 is added is lower than the blade without an endplate. Furthermore, ED1 also consumed extra energy where the negative region C_p is higher. To optimally suppress tip vortices, the lateral distance from the low-pressure side of an endplate must be large enough to prevent the flow from crossing over [15]. However, the lateral distance of ED1 is relatively smaller than ED2 and ED3. Therefore, the selection of an endplate is crucial to ensure that the loss of power due to the additional drag created by the endplate is not more than the additional positive power recovered.

(a) No endplate

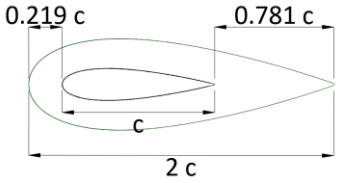

(b) Endplate design 1 (ED1)
endplate profile = NACA 0030

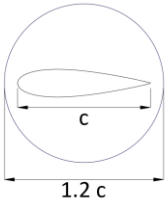

(c) Endplate design 2 (ED2)
endplate profile = circular

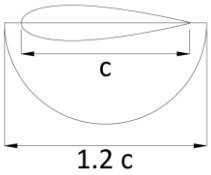

(d) Endplate design 3 (ED3)
endplate profile = semi-circular inward

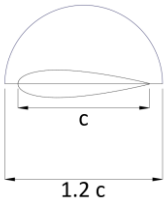

(e) Endplate design 3 (ED4)
endplate profile = semi-circular outward

Fig. 3. Various blade tip designs

Table 1
Summary of the total C_p with four endplate designs, ED1, ED2, ED3, and ED4.

Blade design	TSR					
	1.38		2.19		2.58	
	Total C_p	Improvement	Total C_p	Improvement	Total C_p	Improvement
Baseline - no endplate	0.11455	-	0.31736	-	0.30315	-
ED1	0.09188	-19.79 %	0.29603	-6.72 %	0.29262	-3.47 %
ED2	0.07886	-31.16 %	0.32183	+1.41 %	0.32501	+7.21 %
ED3	0.10159	-11.31 %	0.34102	+7.45 %	0.32070	+5.79 %
ED4	0.10950	-4.41 %	0.32292	+1.75 %	0.30440	+0.42 %

Table 2
Summary of the blade 1 C_p with four endplate designs, ED1, ED2, ED3, and ED4.

Blade design	TSR								
	1.38			2.19			2.58		
	Positive region C_p	Negative region C_p	Average blade 1 C_p	Positive region C_p	Negative region C_p	Average blade 1 C_p	Positive region C_p	Negative region C_p	Average blade 1 C_p
Baseline - no endplate	0.06608	-0.01067	0.05694	0.18608	-0.04301	0.15879	0.17996	-0.06175	0.15117
ED1	0.05475	-0.01751	0.04614	0.17513	-0.06038	0.14708	0.17605	-0.09620	0.14362
ED2	0.04689	-0.019696	0.03894	0.19051	-0.06160	0.16048	0.19702	-0.08975	0.16286
ED3	0.05971	-0.01245	0.05111	0.19934	-0.04541	0.17019	0.19145	-0.07251	0.16
ED4	0.06436	-0.01615	0.05477	0.19011	-0.04889	0.16165	0.18284	-0.07395	0.15225

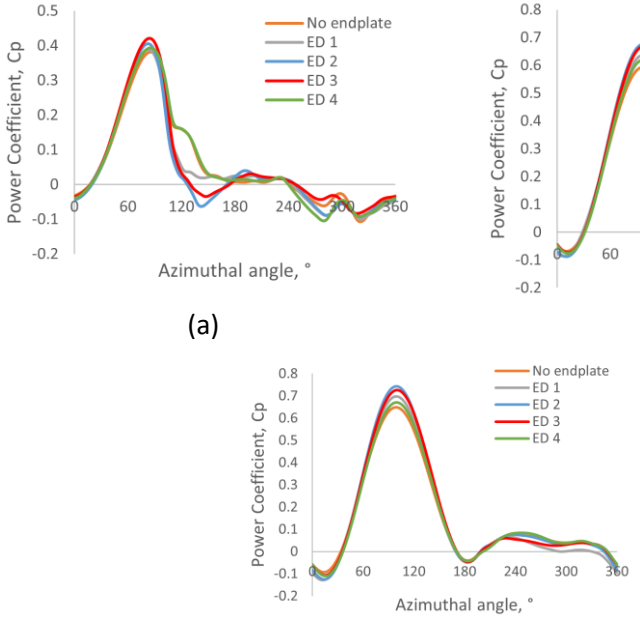

Fig. 4. Comparison of C_p for the single-bladed VAWT with different endplate designs for a complete revolution at the *TSR*s of (a) 1.38, (b) 2.19, (c) 2.58

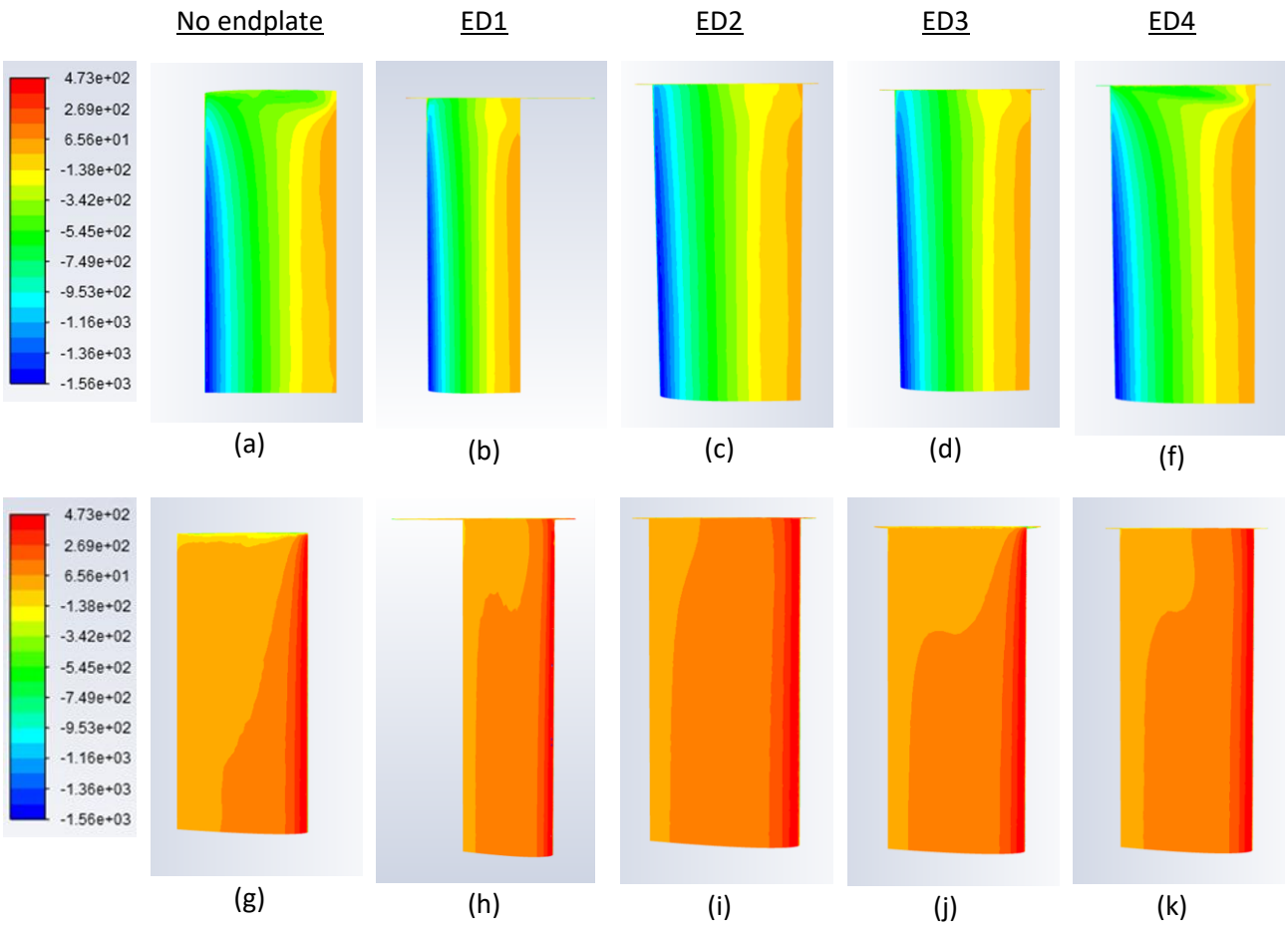

Fig. 5. Comparison of pressure distribution on the blade at the azimuthal angle of 90° at the *TSR* of 2.58. Images (a) to (f) show the low-pressure side, whereas images (g) to (k) show the high-pressure side.

5. Conclusion

In this paper, the effects of four different endplate designs were investigated via 3D CFD simulations. From the investigation, the most suitable endplate design was identified. Based on the results presented in this paper, it was found that ED3 is suitable to apply at the *TSR*s of 2.19 and 2.58 where it showed improvement to the tested conditions. The findings obtained supported that the increase in *Cp* for a VAWT with endplates is due to the success in minimizing the formation of tip vortices. Essentially, the endplate should have sufficient lateral distance at the low-pressure side of the blade to effectively prevent the flow from crossing over to the opposite side to form tip vortices. Nevertheless, further studies are required to understand the relationship between the additional drag created by the endplate and the induced drag that can be recovered by the endplate in order to determine the optimum endplate size. However, the tested endplate designs were unable to show improvement in the VAWT power performance at the *TSR* of 1.38. Further evaluation will require a higher-order turbulence model to capture the dynamic stall in order to obtain a more accurate prediction.

Acknowledgement
This research was funded by the UTM-ER grant (Vot No. 20J89) of Universiti Teknologi Malaysia.

References

[1] Muhammad ArshadBrendan O'Kelly. "Global status of wind power generation: theory, practice, and challenges." *International Journal of Green Energy* 16, no. 14 (2019): 1073-1090. https://doi.org/10.1080/15435075.2019.1597369

[2] E. Kavak AkpinarS. Akpinar. "A statistical analysis of wind speed data used in installation of wind energy conversion systems." *Energy Conversion and Management* 46, no. 4 (2005): 515-532. https://doi.org/10.1016/j.enconman.2004.05.002

[3] Gerald Müller, Mark F. Jentsch, and Euan Stoddart. "Vertical axis resistance type wind turbines for use in buildings." *Renewable Energy* 34, no. 5 (2009): 1407-1412. https://doi.org/10.1016/j.renene.2008.10.008

[4] Aierken Dilimulati, Ted Stathopoulos, and Marius Paraschivoiu. "Wind turbine designs for urban applications: A case study of shrouded diffuser casing for turbines." *Journal of Wind Engineering and Industrial Aerodynamics* 175 (2018): 179-192. https://doi.org/10.1016/j.jweia.2018.01.003

[5] Dominicus Danardono Dwi Prija Tjahjana, Syamsul Hadi, Yoga Arob Wicaksono, Diniar Mungil Kurniawati, Fahrudin Fahrudin, Ilham Satrio Utomo, Sukmaji Indro Cahyono, and Ari Prasetyo. "Study on performance improvement of the Savonius wind turbine for Urban Power System with Omni-Directional Guide Vane (ODGV)." *Journal of Advanced Research in Fluid Mechanics and Thermal Sciences* 55, no. 1 (2019): 126-135.

[6] Firdaus Nofirman, Prasetyo Bambang Teguh, Ab-Samat Hasnida, Prayudi, Hendri, Wahirom, Suyanto Heri, and Halim Rusjdi. "Wind Energy Potential on A Highrise Building: A Preliminary Study." *Journal of Advanced Research in Fluid Mechanics and Thermal Sciences* 88, no. 3 (2021): 20-30. https://doi.org/10.37934/arfmts.88.3.2030

[7] Ismail Ainaa Maya Munira, Ali Zurriati Mohd, Isa Kamariah Md, Abdullah Mohammad, and Zawawi Fazila Mohd. "Study On the Potentiality of Power Generation from Exhaust Air Energy Recovery Wind Turbine: A Review." *Journal of Advanced Research in Fluid Mechanics and Thermal Sciences* 87, no. 3 (2021): 148-171. https://doi.org/10.37934/arfmts.87.3.148171

[8] Qing'an Li, Takao Maeda, Yasunari Kamada, Junsuke Murata, Toshiaki Kawabata, Kento Shimizu, Tatsuhiko Ogasawara, Alisa Nakai, and Takuji Kasuya. "Wind tunnel and numerical study of a straight-bladed vertical axis wind turbine in three-dimensional analysis (Part I: For predicting aerodynamic loads and performance)." *Energy* 106 (2016): 443-452. https://doi.org/10.1016/j.energy.2016.03.089

[9] Rémi Gosselin, Guy Dumas, and Matthieu Boudreau. "Parametric study of H-Darrieus vertical-axis turbines using CFD simulations." *Journal of Renewable and Sustainable Energy* 8, no. 5 (2016): 053301. https://doi.org/10.1063/1.4963240

[10] Stefania ZanforlinStefano Deluca. "Effects of the Reynolds number and the tip losses on the optimal aspect ratio of straight-bladed Vertical Axis Wind Turbines." *Energy* 148 (2018): 179-195. https://doi.org/10.1016/j.energy.2018.01.132

[11] Thomas KinseyGuy Dumas. "Three-Dimensional Effects on an Oscillating-Foil Hydrokinetic Turbine." *Journal of Fluids Engineering* 134, no. 7 (2012): https://doi.org/10.1115/1.4006914

[12] Thierry Villeneuve, Matthieu Boudreau, and Guy Dumas. "Lift enhancement and drag reduction of lifting blades through the use of end-plates and detached end-plates." *Journal of Wind Engineering and Industrial Aerodynamics* 184 (2019): 391-404. https://doi.org/10.1016/j.jweia.2018.12.006

[13] Daegyoum Kim, Benjamin Strom, Shreyas Mandre, and Kenneth Breuer. "Energy harvesting performance and flow structure of an oscillating hydrofoil with finite span." *Journal of Fluids and Structures* 70 (2017): 314-326. https://doi.org/10.1016/j.jfluidstructs.2017.02.004

[14] Nishant Mishra, Anand Sagar Gupta, Jishnav Dawar, Alok Kumar, and Santanu Mitra. "Numerical and Experimental Study on Performance Enhancement of Darrieus Vertical Axis Wind Turbine With Wingtip Devices." *Journal of Energy Resources Technology* 140, no. 12 (2018): https://doi.org/10.1115/1.4040506

[15] Yu Xie, Haigui Kang, Bing Chen, and Wei Guo. "Research on the end-plate for vertical axis tidal current turbine." *Proceedings of the Institution of Mechanical Engineers, Part M: Journal of Engineering for the Maritime Environment* 231, no. 3 (2016): 750-759. https://doi.org/10.1177/1475090216681259

[16] Thierry Villeneuve, Matthieu Boudreau, and Guy Dumas. "Improving the efficiency and the wake recovery rate of vertical-axis turbines using detached end-plates." *Renewable Energy* 150 (2020): 31-45. https://doi.org/10.1016/j.renene.2019.12.088

[17] Seiji Yamada, Tomohiro Tamura, and Shinsuke Mochizuki. "Effects of end plates on performance of a small straight-bladed vertical axis wind turbine." *Journal of Fluid Science and Technology* 12, no. 2 (2017): JFST0019-JFST0019. https://doi.org/10.1299/jfst.2017jfst0019

[18] K Rajaguru NathanS Thanigaiarasu. *Effect of different endplates on blade aerodynamic performance and blade loading of VAWT with symmetric airfoil blades*. in *2017 International Conference on Green Energy and Applications (ICGEA)*. 2017. IEEE. https://doi.org/10.1109/icgea.2017.7924645

[19] GW Rawlings, M Alidadi, VR Klaptocz, Y Nabavi, Y Li, J Mikkelsen, and SM Calisal. *Application of end plates for vertical axis hydro turbine performance enhancement*. in *The Eighteenth International Offshore and Polar Engineering Conference*. 2008. OnePetro.
[20] Richard T Whitcomb, *A design approach and selected wind tunnel results at high subsonic speeds for wing-tip mounted winglets*. 1976.
[21] Marvin P Fink, *Aerodynamic characteristics of low-aspect-ratio wings in close proximity to the ground*. 1961: National Aeronautics and Space Administration.
[22] Yichen Jiang, Chenlu He, Peidong Zhao, and Tiezhi Sun. "Investigation of Blade Tip Shape for Improving VAWT Performance." *Journal of Marine Science and Engineering* 8, no. 3 (2020): https://doi.org/10.3390/jmse8030225
[23] Qing'an Li, Takao Maeda, Yasunari Kamada, Junsuke Murata, Kazuma Furukawa, and Masayuki Yamamoto. "The influence of flow field and aerodynamic forces on a straight-bladed vertical axis wind turbine." *Energy* 111 (2016): 260-271. https://doi.org/10.1016/j.energy.2016.05.129
[24] Kok Hoe Wong, Wen Tong Chong, Sin Chew Poh, Yui-Chuin Shiah, Nazatul Liana Sukiman, and Chin-Tsan Wang. "3D CFD simulation and parametric study of a flat plate deflector for vertical axis wind turbine." *Renewable Energy* 129 (2018): 32-55. https://doi.org/10.1016/j.renene.2018.05.085
[25] Robert Howell, Ning Qin, Jonathan Edwards, and Naveed Durrani. "Wind tunnel and numerical study of a small vertical axis wind turbine." *Renewable energy* 35, no. 2 (2010): 412-422. https://doi.org/10.1016/j.renene.2009.07.025
[26] H. F. LamH. Y. Peng. "Study of wake characteristics of a vertical axis wind turbine by two- and three-dimensional computational fluid dynamics simulations." *Renewable Energy* 90 (2016): 386-398. https://doi.org/10.1016/j.renene.2016.01.011
[27] Mojtaba Tahani, Narek Babayan, Seyedmajid Mehrnia, and Mehran Shadmehri. "A novel heuristic method for optimization of straight blade vertical axis wind turbine." *Energy Conversion and Management* 127 (2016): 461-476. https://doi.org/10.1016/j.enconman.2016.08.094
[28] Abdullah Mobin Chowdhury, Hiromichi Akimoto, and Yutaka Hara. "Comparative CFD analysis of Vertical Axis Wind Turbine in upright and tilted configuration." *Renewable Energy* 85 (2016): 327-337. https://doi.org/10.1016/j.renene.2015.06.037
[29] Jonathan M. Edwards, Louis Angelo Danao, and Robert J. Howell. "PIV measurements and CFD simulation of the performance and flow physics and of a small-scale vertical axis wind turbine." *Wind Energy* 18, no. 2 (2015): 201-217. https://doi.org/10.1002/we.1690
[30] Kok Hoe Wong, Wen Tong Chong, Nazatul Liana Sukiman, Yui-Chuin Shiah, Sin Chew Poh, Kamaruzzaman Sopian, and Wei-Cheng Wang. "Experimental and simulation investigation into the effects of a flat plate deflector on vertical axis wind turbine." *Energy Conversion and Management* 160 (2018): 109-125. https://doi.org/10.1016/j.enconman.2018.01.029
[31] HK VersteegW Malalasekera. "An introdution to computational fluid dynamics." *The finite volume method* (1995):
[32] Agostino De Marco, Domenico P. Coiro, Domenico Cucco, and Fabrizio Nicolosi. "A Numerical Study on a Vertical-Axis Wind Turbine with Inclined Arms." *International Journal of Aerospace Engineering* 2014 (2014): 1-14. https://doi.org/10.1155/2014/180498
[33] Abdolrahim Rezaeiha, Ivo Kalkman, and Bert Blocken. "CFD simulation of a vertical axis wind turbine operating at a moderate tip speed ratio: Guidelines for minimum domain size and azimuthal increment." *Renewable Energy* 107 (2017): 373-385. https://doi.org/10.1016/j.renene.2017.02.006
[34] Carlos Simão Ferreira, Gijs van Kuik, Gerard van Bussel, and Fulvio Scarano. "Visualization by PIV of dynamic stall on a vertical axis wind turbine." *Experiments in Fluids* 46, no. 1 (2008): 97-108. https://doi.org/10.1007/s00348-008-0543-z
[35] Abdolrahim Rezaeiha, Hamid Montazeri, and Bert Blocken. "On the accuracy of turbulence models for CFD simulations of vertical axis wind turbines." *Energy* 180 (2019): 838-857. https://doi.org/10.1016/j.energy.2019.05.053
[36] M. Salman Siddiqui, Naveed Durrani, and Imran Akhtar. "Quantification of the effects of geometric approximations on the performance of a vertical axis wind turbine." *Renewable Energy* 74 (2015): 661-670. https://doi.org/10.1016/j.renene.2014.08.068
[37] Hang Lei, Dai Zhou, Yan Bao, Ye Li, and Zhaolong Han. "Three-dimensional Improved Delayed Detached Eddy Simulation of a two-bladed vertical axis wind turbine." *Energy Conversion and Management* 133 (2017): 235-248. https://doi.org/10.1016/j.enconman.2016.11.067
[38] Weipao Miao, Qingsong Liu, Zifei Xu, Minnan Yue, Chun Li, and Wanfu Zhang. "A comprehensive analysis of blade tip for vertical axis wind turbine: Aerodynamics and the tip loss effect." *Energy Conversion and Management* 253 (2022): https://doi.org/10.1016/j.enconman.2021.115140

[39] Abdolrahim Rezaeiha, Hamid Montazeri, and Bert Blocken. "CFD analysis of dynamic stall on vertical axis wind turbines using Scale-Adaptive Simulation (SAS): Comparison against URANS and hybrid RANS/LES." *Energy Conversion and Management* 196 (2019): 1282-1298. https://doi.org/10.1016/j.enconman.2019.06.081

[40] Ye LiSander M. Calisal. "Three-dimensional effects and arm effects on modeling a vertical axis tidal current turbine." *Renewable Energy* 35, no. 10 (2010): 2325-2334. https://doi.org/10.1016/j.renene.2010.03.002